UMT PRESS

Journal of Sustainability Science and Management
Journal Homepage: https://jssm.umt.edu.my
eISSN: 2672-7226
DOI: http://doi.org/10.46754/jssm.2026.06.009

INVESTIGATION OF CARBOXYMETHYL CELLULOSE (CMC) AS A SUSTAINABLE CORROSION INHIBITOR FOR MILD STEEL IN SEAWATER

WAN MOHD NORSANI WAN NIK[1], ADI HAFIZAMRI ARIFFIN[1], NUR FATIHAH HAMDAN KUMARAN[1], SURIANI MAT JUSOH[1], VINCENT ONUEGBU IZIONWORU[2], MOHD AZLAN MUSA[1] AND MOHAMMAD FAKHRATUL RIDWAN ZULKIFLI[1]*

[1]Marine Materials Research Group, Faculty of Ocean Engineering Technology, Universiti Malaysia Terengganu, 21030 Kuala Nerus, Terengganu, Malaysia
[2]Department of Chemical and Petrochemical Engineering, Rivers State University, Nkpolu-Oroworukwo, Port Harcourt, Nigeria

**Corresponding author: fakhratulz@umt.edu.my*

ARTICLE INFO

Article History:
Received: 16 March 2025
Revised: 28 December 2025
Accepted: 2 April 2026
Published: 15 June 2026

Keywords:
Carboxymethyl cellulose, recurrent neural network, mild steel, EIS

ABSTRACT

Corrosion significantly hampers the application of mild steel in marine environments, demanding highly efficient and sustainable corrosion inhibitors. Conventional inhibitors often pose environmental and health risks, underscoring the urgent need for green, non-toxic alternatives. This study investigates the efficacy of carboxymethyl cellulose (CMC) as an environmentally friendly corrosion inhibitor for mild steel in seawater. The methodology involved Fourier Transform Infrared Spectroscopy (FTIR) to classify functional groups while Electrochemical Impedance Spectroscopy (EIS) and Potentiodynamic Polarisation (PdP) to evaluate corrosion inhibition efficiency. FTIR confirmed critical molecular interactions enabling cellulose dissolution and enhanced inhibitor performance in CMC, Ionic Liquid (IL), and Cellulose Ionic Liquid (CIL), highlighting molecular interactions that help cellulose dissolution in IL, facilitated by hydrogen bonding and metal complex formation through nitrogen atom's lone-pair electrons. EIS revealed outstanding inhibition efficiency of up to 94%, marking a significant inhibitory effect. PdP validated the dual anodic-cathodic suppression, achieving up to 92% efficiency with optimal performance at 40 to 60 ppm. Predictive analysis using Recurrent Neural Networks (RNN) indicated that GRU outperforms LSTM as the RMSE is lower by approximately 3.81 units. It emphasises the suitability of this model for modelling impedance behaviour in this study. Overall, these findings establish CMC as a highly promising sustainable inhibitor, offering substantial protection for mild steel in marine application and advancing the integration of green chemistry with intelligent computational modelling.

Introduction

Mild steel is a widely employed material in marine industries and equipment manufacturing globally such as shipbuilding, offshore, and power plant. Its affordability, durability, hardness, and ease of fabrication, make it a preferred choice for producing equipment components. However, a major limitation of mild steel in industrial applications is its tendency to undergo corrosion (Habeeb *et al.*, 2018). This issue continues to pose a significant challenge for corrosion specialist (Abdel-Gaber *et al.*, 2020). Corrosion in seawater

environments is particularly aggressive attributable to the chloride ions, which accelerate the electrochemical reactions, leading to metal degradation. It is a major concern for industries like shipping, offshore oil and gas, and coastal infrastructure due to the high salinity, oxygen content, and biological activity in seawater. Several studies have confirmed that chloride ions in seawater accelerate both anodic and cathodic reactions, leading to rapid deterioration of mild steel surfaces. Khamis *et al*. (2016) demonstrated through electrochemical impedance spectroscopy that seawater exposure results in significant charge transfer processes. To mitigate this problem, corrosion inhibitors are widely used in the marine industry as an economical and environmentally friendly approach to corrosion control (Haque *et al.*, 2023).

These inhibitors are chemicals introduced into a corrosion system to mitigate the corrosion rate of metal equipment (Olajire, 2017). Several categories of corrosion inhibitors exist including organic inhibitors, inorganic inhibitors, and mixed inhibitors. Inorganic inhibitors are frequently applied to control corrosion, but they are typically associated with toxicity (Hossain *et al.*, 2021). A significant issue with conventional inhibitors is their potential harm to both the environment and human health, as many are nondegradable and poisonous. To mitigate these risks, strict international regulations must be enforced to control the use of harmful inhibitors (Koch *et al.*, 2016). Organic green corrosion inhibitors, which should match the efficacy of conventional inhibitor in reducing corrosion rates and protecting metal, offer a more sustainable alternative (Reza *et al.*, 2021; Nik *et al.*, 2023). Biopolymers such as starch, chitosan, and cellulose derivatives have been widely investigated as eco-friendly inhibitors due to their biodegradability and strong adsorption capacity. Abdel-Gaber *et al*. (2020) reported that natural polysaccharides effectively reduce corrosion rates of mild steel in chloride-rich environments, while Huang *et al*. (2022) highlighted that cellulose-based inhibitors provide comparable efficiency to conventional synthetic inhibitors without environmental drawbacks.

Carboxymethyl cellulose (CMC) is an effective organic corrosion inhibitor, widely recognised for its environmentally friendly properties (Verma *et al.*, 2024). CMC has attracted significant interest due to its unique chemical structure, which features several polar functional groups such as carboxyl and hydroxyl groups, enhancing its adsorption capacity (Rahman *et al.*, 2021). Additionally, CMC, as an anionic environmentally friendly polymer, offers further advantages such as low cost, non-toxicity, and water solubility (Akhlaq *et al.*, 2023). CMC is also known for its biodegradability, enhancing adsorption onto metal surfaces and functions as both thermodynamic and kinetic inhibitor, depending on its molecular weight and formulation (Macedo *et al.*, 2019; Voloshin *et al.*, 2021).

Machine learning serves as a valuable tool for predictive analysis, offering significant advantages over relying solely on experimental data (Zhong *et al.*, 2021). For instance, a specific type of artificial neural network known as Recurrent Neural Networks (RNNs) are established to cater time series data or sequential data. RNNs are trained to generate predictions at each time step by utilising current input and information from previous time steps. For example, RNNs have been utilised to predict polarisation resistance trends (Huang *et al.*, 2022), while Thiyagalingam *et al*. (2022) emphasised the role of deep learning in reducing experimental workload.

In this study, CMC was chosen as a corrosion inhibitor, mild steel was used as a substrate, and seawater was opted as a corrosion media. Mild steel was selected as the substrate in this study because of its widespread use in shipbuilding, offshore structures, and power plant components where cost effectiveness and mechanical strength are critical while seawater was opted as a corrosive medium due to its aggressiveness towards steel corrosion. The inhibitive behaviour of CMC was characterised via Electrochemical Impedance Spectroscopy

(EIS). The EIS data were then used to predict real impedance through the application of Recurrent Neural Networks (RNNs). Two specific architectures, Long Short-term Memory (LSTM) and Gated Recurrent Unit (GRU) were employed in this predictive analysis. The novelty of this work lies in the integration of a sustainable corrosion inhibitor with advanced recurrent neural network architecture (LSTM and GRU) to predict real impedance behaviour from EIS data, underscoring its importance in bridging green materials research with intelligent computational modelling.

Materials and Methods

Mild Steel Preparation

The test specimens, composed of mild steel with dimensions of 25 mm × 25 mm × 3 mm were employed as substrates in the solution. Mild steel surfaces were polished using a grinding and polishing machine with emery papers of grit sizes 80, 120, 240, 360, 600, and 1,000. Subsequently, the specimens were cleaned with acetone and rinsed with distilled water. Finally, the samples were dried and stored in a desiccator.

Preparation of CMC as a Corrosion Inhibitor

Numerous researchers have proposed methods that combine environmentally friendly solvents with biodegradable materials to benefit both the environment and consumers (Zhang *et al.*, 2021). In this experiment, CMC, a natural polymer was dissolved in the ionic liquid solvent, 1-ethyl-3-methylimidazolium acetate (EMIMAc) to enhance its solubility in seawater. The resulting compound, hereafter referred to as carboxy methylcellulose-ionic liquid (CIL) was subsequently employed as a corrosion inhibitor for mild steel in seawater. CMC powder was sourced from a local company, while the EMIMAc ionic liquid was procured from Sigma Aldrich without further processing. CMC was continuously stirred with EMIMAc at 60°C for 30 minutes. The final product was employed as a corrosion inhibitor for mild steel, tested in seawater at concentrations ranging from 20 to 80 ppm.

Fourier Transform Infrared (FTIR) Spectroscopy

In this study, Bruker-INVENIO Fourier Transform Infrared (FTIR) spectroscopy was used in identifying the functional groups of CMC, EMIMAc, and the CMC product after dissolution in EMIMAc. The compound was placed in the sample holder, and the instrument was initialised to allow infrared light to pass through the sample over a wavelength range of 400 to 4000 cm^{-1} with a spectral resolution of 4 cm^{-1}. This process generated a spectrum representing the molecular composition of the tested compounds. Specific peaks and patterns in the resulting spectrum were analysed to identify the functional groups present in the compound. A molecular structure of CMC and EMIMAc were constructed using Chemical Sketch Tool which available freely on the following website, rcsb.org.

Electrochemical Impedance Spectroscopy (EIS)

Electrochemical Impedance Spectroscopy (EIS) is an instrument used to analyse electrochemical systems by examining their responses to a repetitive, low-amplitude Alternating Current (AC) signal. Analysing the system's response yields important insights into the structure and behaviour of the interface (Lazanas & Prodromidis, 2023). The electrochemical analysis of corrosion inhibition on the mild steel interface, both in the presence and absence of CMC in seawater was conducted using the Gamry 1010E EIS. Prior to EIS characterisation, the specimens were immersed in seawater with and without CMC for two hours to achieve a steady-state potential. A standard three-electrode configuration was used, with mild steel as the working electrode, a silver wire coated in Ag/AgCl as the reference electrode, and a platinum rod as the counter electrode. The EIS frequency range was set from 0.1 to 100,000 Hz, and the alternating current voltage perturbation was set to 10 mV (PourghasemiHanza *et al.*, 2021). Electrochemical circuit fitting was performed once the Nyquist plot obtained from the

experimental procedure using Gamry 1010E EChem Analyst software. A simple Randles circuit was used to fit the electrochemical data to achieve polarisation resistance, R_p (Zhang *et al.*, 2024). The R_p value was used to calculate the Inhibition Efficiency (IE) based on the following equation (Wadhwani *et al.*, 2016).

$$IE\ (\%) = \frac{R_p inhibited - R_p uninhibited}{R_p inhibited} \times 100\% \quad (1)$$

Potentiodynamic Polarisation (PdP)

A scan rate of 1 mV/s was used to scan the potential for PdP from -250 mV to +250 mV. This scan rate was chosen because it provides a balance between accuracy and stability, allowing sufficient time for the system to reach a steady state, which ensures reliable measurements of corrosion parameters.

Recurrent Neural Network (RNN)

The obtained Nyquist data from EIS was used as an input and output for prediction purposes using MATLAB R2023a software, the dataset was divided into training and test data with 90% of the sequence allocated for training and the remaining 10% for testing. To enhance compatibility and avoid divergence during training, the training data were standardised to have zero mean and unit variance. To predict future time step values in a sequence, the responses were defined as the training sequences with values shifted by one time step. At each time step of the input sequence, the LSTM/GRU network was trained to forecast the next time step's value, using the training sequences excluding the final time step as predictors. Before utilising Deep Network Designer for training the dataset, the training data were transformed into a datastore object. Deep Network Designer was then utilised to create the LSTM/GRU network architecture, as depicted in Figure 1 (a) and (b). The properties of the layers were adjusted to suit the impedance dataset. The solver for the network architecture was set to Adam, with an initial learning rate of 0.005 and a maximum of 500 epochs. The gradient threshold was fixed at one to avoid gradient explosion (Ghimire *et al.*, 2022; Lipu *et al.*, 2022).

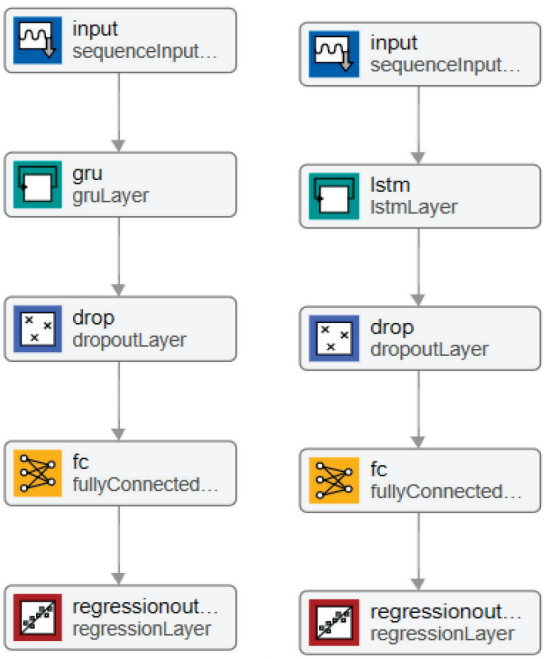

(a) (b)

Figure 1: Network architecture employed in deep network designer for (a) GRU and (b) LSTM

Results and Discussion

Fourier Transform Infrared (FTIR) Spectroscopy

The FTIR spectra for pure CMC were observed in the fingerprint region and matched those in the Spectra Library. The broad peak at 3,445 cm^{-1} is attributed to the hydroxyl group (-OH) as depicted in Figure 2 (a). A strong, sharp absorption peak was noted at 1,586 cm^{-1}, indicating the anti-symmetric and symmetric stretching vibrations of the carboxylate group (COO-). An absorption band at 1,412 cm^{-1} corresponds to the bending vibration mode of the hydroxyl group (OH). The peak at 1,322 cm^{-1} is assigned to the stretching vibration of the C–H bond, while the peak at 1,061 cm^{-1} corresponds to the C–O–C stretching vibration (El-Sakhawy *et al.*, 2018; Sohaimy *et al.*, 2022).

The IR spectral bands for EMIMAc ranging from 2,893 to 3,161 cm^{-1} correspond to the C–H vibrational modes of the imidazolium ring as depicted in Figure 2 (b). The IR spectral bands at 1,573 cm^{-1} correspond to the C=N aromatic group (Kim, 2023). The IR spectra at 1,326 cm^{-1} and is due to C–N stretching vibrations from acetate, respectively. The IR bands seem at 1,174 cm^{-1} and 1,040 cm^{-1} are due to ring in-plane asymmetric stretching of $[Emim]^+$ cation (contributions from the $(N)CH_2$, $CH_3(N)$ CN, and C–C stretching) and C–O stretching vibrations, respectively. The spectral IR bands obtained at 900 cm^{-1} and 625 cm^{-1} correspond to aromatic C–H bending vibrations and C–H bending vibrations (Yesudass *et al.*, 2016).

The cellulose ionic liquid is the combination of carboxymethyl cellulose and 1-ethyl-3-methylimidazolium acetate, which is an ionic liquid. It displays a notable peak at 3,346 cm^{-1} corresponding to a stretching vibration of the O–H (hydroxyl) group as depicted in Figure 2 (c). The IR spectral at 1,560 cm^{-1} is due to the C=N aromatic group which shifted from the original EMIMAc at 1,573 cm^{-1}. The IR bands at 1,380 cm^{-1} and 1,170 cm^{-1} are due to the C–N stretching and symmetric stretching vibration of C–OC– in CMC. The IR spectra at 759 cm^{-1} and 612 cm^{-1} correspond to C–H rocking vibrations and C–H bending vibrations, respectively (Ariffin *et al.*, 2024).

The molecular framework of cellulose as illustrated in Figure 2 (a), highlights the presence of hydrogen and oxygen atoms which involve in donor-acceptor interactions with the charge components of imidazolium Ionic Liquids (ILs). These interactions predominantly occur at the C-6 and C-3 hydroxyl groups of adjacent cellulose chains. As a result, the hydroxyl group become dissociated, which promotes the dissolution of cellulose in imidazolium-based ILs. The remarkable solubility of cellulose in these solvents stems from the ability of ILs to break apart the extensive hydrogen-bonding network that stabilises the cellulose structure. This process can be further enhanced by the high chloride concentration found within the imidazolium IL framework. As illustrated in Figure 2 (b), the nitrogen atom's lone-pair electrons act as coordination sites for metal complex formation, facilitating interactions with the metal ions in the studied material. Consequently, the adsorption process of CIL onto the metal substrate can be elucidated through the lens of these metal complexation formations (Arora, 2019; Saheed *et al.*, 2022). A summary of the IR spectra for CMC, EMIMAc, and CIL is tabulated in Table 1.

Electrochemical Impedance Spectroscopy (EIS)

By examining the curve shapes of the Nyquist plot, as illustrated in Figure 3, we observed that the curves can be approximated by a single capacitive semicircle. The plot exhibits a nearly perfect semicircle, suggesting that the electrochemical process is primarily controlled by the charge transfer mechanism (Ariffin *et al.*, 2024). Charge transfer refers to the disparity in the real impedance axis between low and high frequency domains for all samples, the

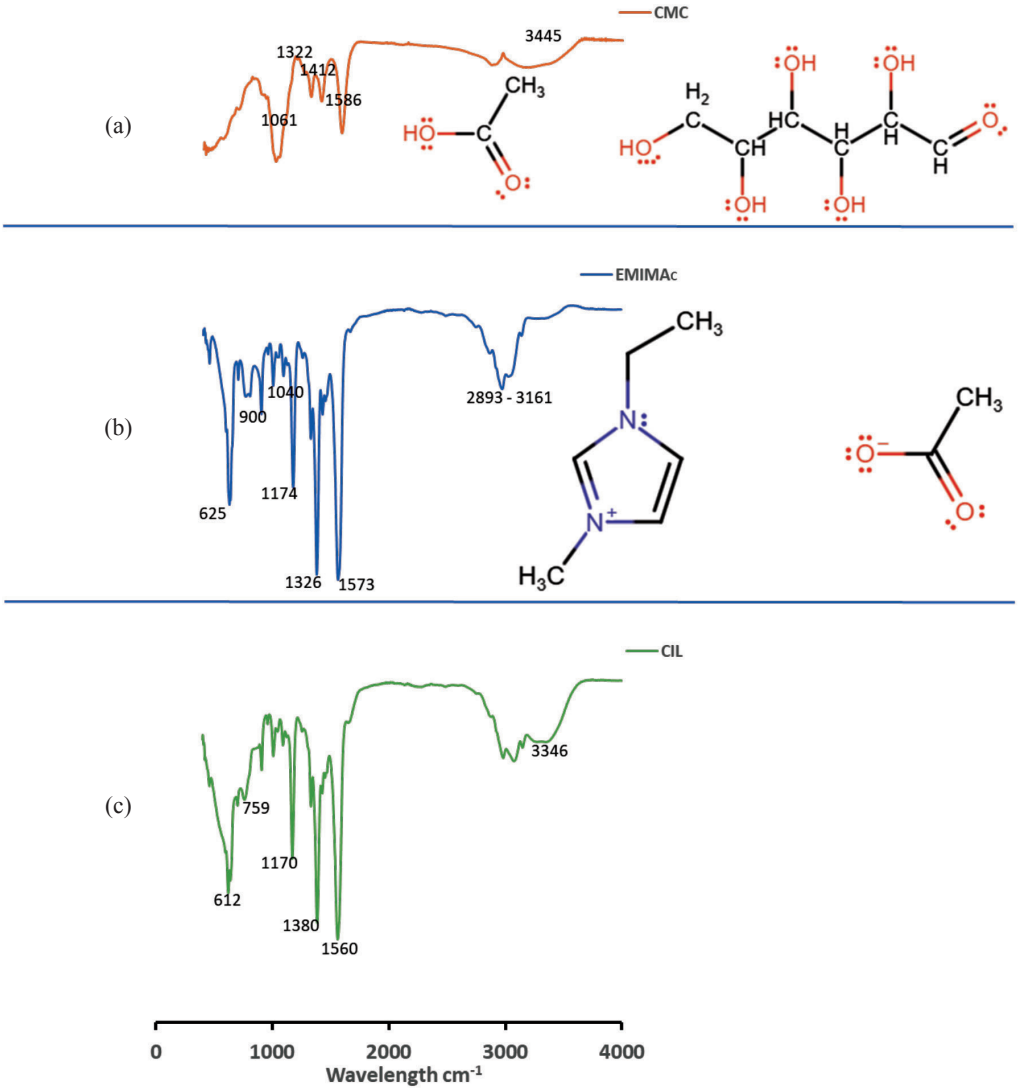

Figure 2: IR spectrum obtained for (a) CMC, (b) EMIMAc, and (c) CIL

Table 1: Summary of IR Spectra for CMC, EMIMAc, and CIL

Material	Wavenumber (cm^{-1})	Functional Group/ Vibration	Description
CMC	3,445	O–H stretching	Broad peak indicating hydroxyl groups
	1,586	COO^- asymmetric/ symmetric stretching	Carboxylate group
	1,412	O–H bending	Hydroxyl bending mode
	1,322	C–H stretching	Aliphatic stretching vibration
	1,061	C–O–C stretching	Ether linkage from cellulose backbone

EMIMAc	2,893–3,161	C–H stretching	Vibrations from imidazolium ring
	1,573	C=N aromatic stretching	Imidazolium ring signature
	1,326	C–N stretching (acetate)	Indicates IL side-chain bonding
	1,174; 1,040	Ring in-plane asymmetric and C–O stretching	$[Emim]^+$ cation ring and acetate anion contributions
	900; 625	Aromatic C–H bending	Imidazolium ring bending modes
CIL	3,346	O–H stretching	Slightly shifted hydroxyl group due to interaction with IL
	1,560	C=N aromatic stretching	Shifted from original EMIMAc, indicating complexation
	1,380	C–N stretching	Corresponds to EMIMAc interaction
	1,170	Symmetric C–O–C stretching	Indicates CMC backbone preserved within IL matrix
	759; 612	C–H rocking and bending	Additional shifts due to complexation and hydrogen bond disruption

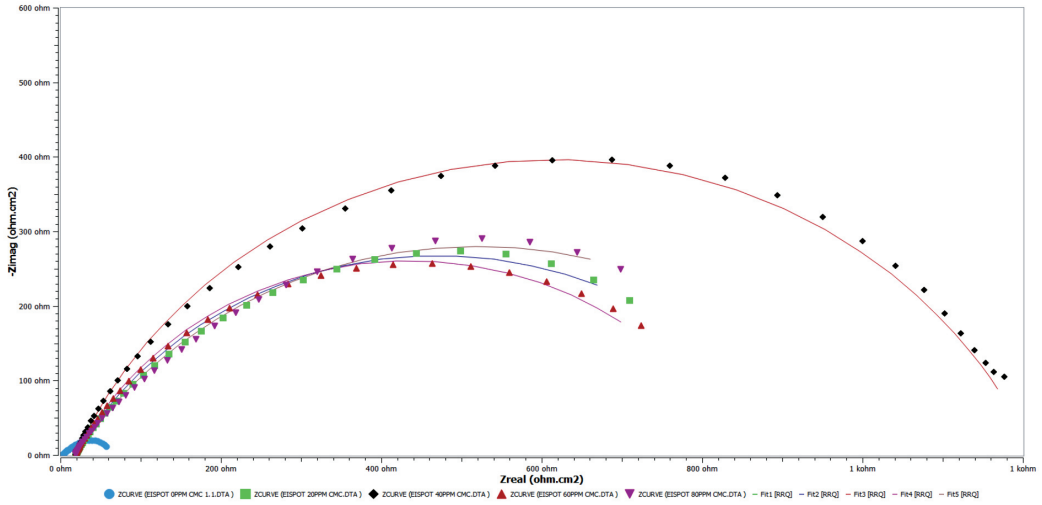

Figure 3: Nyquist curve of inhibited and uninhibited mild steel

curve shapes remained consistent throughout the testing period, indicating that neither the immersion duration nor the addition of the inhibitor significantly altered the corrosion process (Pruthviraj, 2016).

At 0 ppm, the polarisation resistance (R_p) value is measured at 72.31 Ω cm², establishing a baseline for mild steel in seawater without any corrosion inhibitor as tabulated in Table 2. When the concentration is increased to 20 ppm, the R_p value rises significantly to 903.30 Ω cm², demonstrating a marked enhancement in corrosion resistance due to the introduction of a modest amount of the inhibitor. At 40 ppm, the R_p value peaks at 1,196.10 Ω cm², indicating that this concentration offers the most effective corrosion inhibition within the tested range. However, at 60 ppm, the R_p value experiences a slight decline to 833.31 Ω cm², suggesting a potential decrease in corrosion inhibition efficiency at higher concentrations. This phenomenon could be attributed by several reasons such as the film may become unstable or less effective due to saturation or agglomeration

of inhibitor molecules, leading to a drop in R_p (Anita *et al*., 2023), complex electrochemical interactions, including the formation of secondary phases or precipitates that may not contribute effectively to corrosion protection (Pine Research Instrumentation, 2016), and formation of a more stable and effective protective film, or the inhibitor molecules may reorganise into a more efficient configuration, causing R_p to rebound (Umoren *et al*., 2018).

Conversely, at 80 ppm, the R_p value rebounds to 1,003.50 Ω cm², reflecting an improvement in corrosion resistance, although it remains lower than the level observed at 40 ppm. In summary, the data indicate that the concentration of the corrosion inhibitor substantially affects the R_p value. The greatest resistance to corrosion is recorded at a concentration of 40 ppm, while higher concentrations exhibit varying degrees of effectiveness. This suggests the existence of an optimal concentration range for the corrosion inhibitor to attain the most favourable outcomes.

The CPE value is measured at 8 mF at 0 ppm, establishing a baseline for mild steel in seawater without any corrosion inhibitor. When the concentration is increased to 20 ppm, the CPE value slightly decreases to 0.7 mF, indicating a reduction in the system's capacitive behaviour with the introduction of a low concentration of the inhibitor. At 40 ppm, the CPE value further declines to 0.3 mF, suggesting a significant alteration in the electrochemical behaviour and an enhancement in corrosion inhibition. At 60 ppm, the CPE value increases to 0.60 mF and by 80 ppm, the CPE value further increases to 0.9 mF. A slight increase at higher concentrations could occur due to the rearrangement of the adsorbed layer on the metal surface (El-Housseiny *et al*., 2022). The observed decreases in CPE with increasing CMC concentration indicates effective adsorption and protective film formation on mild steel, thereby reducing the active surface area for charge transfer. This trend is consistent with previous finding by Abdel-Gaber *et al*. (2024) who demonstrated that eco-friendly inhibitors lower CPE values by enhancing barrier properties and capacitive behaviour at the steel-solution.

Equivalent circuit models offer valuable insights into the significance of impedance parameter variations derived from Electrochemical Impedance Spectroscopy (EIS) spectra. The circuit model utilised for fitting the experimental data of the inhibiting system, as illustrated in Figure 4, comprises a parallel element of charge transfer resistance (R_{ct}) and a Constant Phase Element (CPE), representing the adsorption mechanism of the inhibitor and the metal substrate. A single-loop semicircle plot was fitted with an RRQ circuit model, consisting of a resistor in series with a parallel arrangement of another resistor and a constant phase element, as frequently reported in earlier studies (Umoren *et al*., 2018, Zulkifli *et al*., 2021).

A slight reduction in effectiveness was observed, potentially due to the destabilisation of the protective film at elevated concentrations. The variation in concentration suggests that the electrochemical changes indicate a suppression of the corrosion process at higher inhibitor levels (Aslam *et al*., 2022). This takes place when the inhibitors adsorb onto the metal surface, consequently decreasing the active surface area in contact with aggressive corrosive electrolytes.

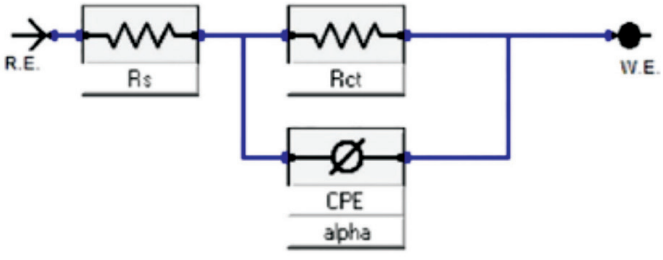

Figure 4: Randle's circuit used for electrochemical data fitting

The molecular structure and adsorption characteristics of Ionic Liquids (ILs) are significant factors in the adsorption process. CILs composed of ions can strongly adsorb onto metal surfaces due to electrostatic interactions between the charged species and the metal. This strong adsorption leads to the development of a stable, compact protective layer that effectively shields the metal from corrosive agents, including air and chloride ions in seawater (Liu *et al.*, 2023). Increased adsorption correlates with enhanced inhibitory efficacy.

In the absence of inhibitor, |Z| shows its lowest point at low frequency, consistent with active corrosion as depicted in Figure 5. The phase angle lies in more positive region and narrower phase region, indicating faster kinetics and a more resistive interface. The addition of CMC altered the electrochemical response of mild steel. The value of |Z| rised consistently with the increasing of concentration, indicating the formation of barrier layer and significant charge transfer suppression and the similar trend has been reported by El-Housseiny *et al*. (2022). The phase angle shows a more negative value and broader bandwidth as CMC is added into the system which indicates that CMC has started to form a protective film and has improved capacitive behaviour (Khamis *et al*., 2025).

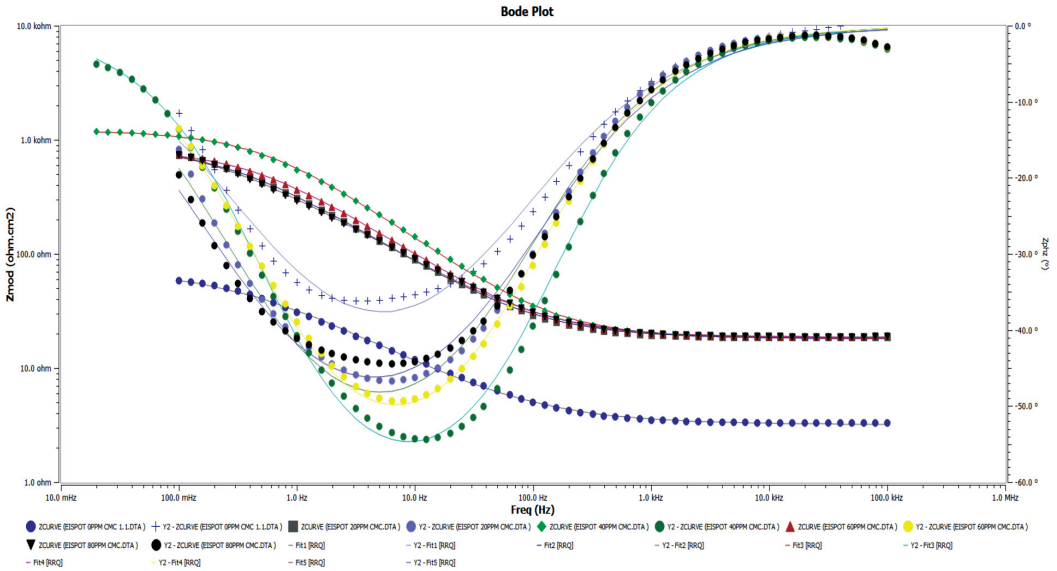

Figure 5: Bode plot of inhibited and uninhibited mild steel

Table 2: Electrochemical parameters obtained from EIS method

Concentration (ppm)	R_p ($\Omega.cm^2$)	R_u ($\Omega.cm^2$)	CPE (mF)	Goodness of Fit	IE (%)
0	72.31	3.19	8.0	$8.86x10^{-4}$	-
20	903.30	18.05	0.7	$7.97x10^{-4}$	92
40	1196.10	18.39	0.3	$6.33x10^{-4}$	94
60	833.31	18.64	0.6	$2.56x10^{-4}$	91
80	1003.50	18.04	0.9	$1.11x10^{-3}$	93

Potentiodynamic Polarisation Resistance

Figure 6 depicts the anodic and cathodic polarisation behaviour of a metal substrate in the absence and presence of varying concentrations of CMC. This electrochemical technique helps quantify the corrosion rate and elucidate the inhibition mechanism.

With the addition of CMC (40 to 80 ppm), the corrosion potential (E_{corr}) shifted slightly in the active region (697.2 to 693.5 mV) compared to the uninhibited sample (682.2 mV), suggesting that the inhibitor primarily influences the cathodic reaction such as hydrogen evolution rather than the anodic metal dissolution (Solmaz *et al.*, 2023). In essence, when CMC adsorbs onto the metal surface, it selectively retards the cathodic sites, thereby reducing their kinetics. As a result, the mixed potential theory predicts a new corrosion potential that's more negative, reflecting a shift in the balance between the anodic and cathodic partial currents. However, despite this negative shift, the overall corrosion current density (i_{corr}) still drops, indicating improved corrosion resistance. A shift towards noble direction is noted for the 20 ppm sample, likely due to the inhibitor primarily affecting the anodic reaction. It may adsorb on anodic sites, delaying metal dissolution more than it suppresses cathodic activity. This suggests anodic inhibition dominance at lower concentrations, where the inhibitor partially blocks oxidation sites but has not formed a uniform surface film yet (Zheng *et al.*, 2023).

Corrosion current density, i_{corr} shows a clear reduction with increasing CMC concentration as tabulated in Table 3. The i_{corr} at 80 ppm is significantly lower than at 0 ppm, confirming superior inhibition performance. This trend indicates that CMC forms a protective barrier,

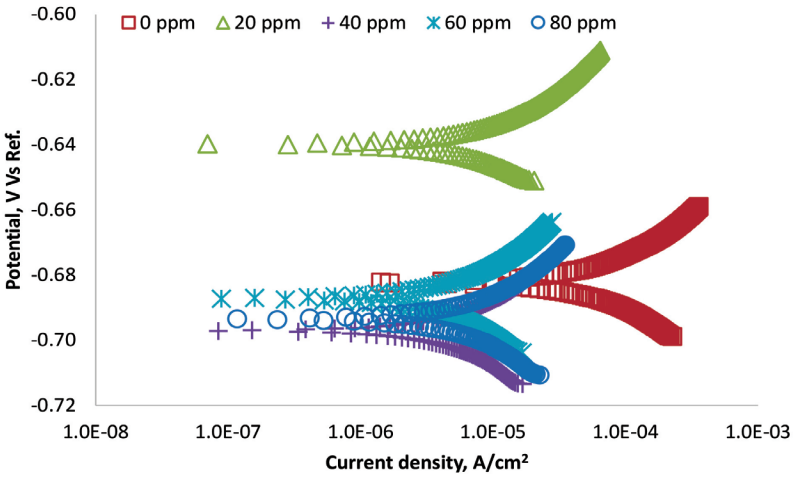

Figure 6: Tafel curve of inhibited and uninhibited mild steel

Table 3: Potentiodynamic polarisation data of inhibited and uninhibited mild steel

Concentration (ppm)	i_{corr} (µA/cm²)	E_{corr} (mV)	R_p (Ω)	Corrosion Rate (mpy)	IE (%)
0	314	-682.2	82.96	143.50	
20	41.96	-639.8	620.8	19.17	87
40	25.72	-697.2	1013	11.75	92
60	24.03	-687.2	1084	10.98	92
80	32.49	-693.5	801.9	14.85	90

hindering both anodic metal dissolution and cathodic hydrogen evolution. CMC likely adsorbs onto the metal substrate via its oxygen-containing functional groups (–COO^-, –OH), forming a physical barrier that blocks electrolyte access to reactive sites. A qualitative estimation of Inhibition Efficiency (IE) reveals that the efficiency increases progressively from 20 ppm to 80 ppm.

The polarisation resistance (R_p) and corrosion rate data clearly demonstrate the effectiveness of CMC in mitigating mild steel corrosion in seawater. In the absence of inhibitor, R_p is very low (82.96 Ω) and the corrosion rate is extremely high (143.50 mpy), reflecting severe corrosion. With the addition of CMC, R_p increases sharply to 620.8 Ω at 20 ppm, accompanied by a drastic reduction in corrosion rate to 19.17 mpy. Further increases in concentration to 40 to 60 ppm yield the highest R_p values (1,013 to 1,084 Ω) and the lowest corrosion rates (11 to 10.98 mpy), indicating optimal inhibition efficiency. At 80 ppm, however, R_p decreases to 801.9 Ω and the corrosion rate rises slightly to 14.85 mpy, suggesting that excessive dosage may reduce stability of uniformity of the protective film.

The potentiodynamic polarisation plot conclusively demonstrates that CMC acts as an effective corrosion inhibitor in a concentration-dependent manner. The optimal performance appears at 40 to 60 ppm, where corrosion is most significantly mitigated. The data suggest that CMC functions as a mixed-type inhibitor, primarily through adsorptive film formation, reducing both anodic and cathodic reactions without drastically altering the underlying mechanisms.

Recurrent Neural Network (RNN)

The Recurrent Neural Network (RNN) model utilises Z real and Z imaginary data, which consists of single time series data, as the input layer for this prediction model. Here, time steps correspond to Z real, while values relate to the number of Z imaginary. Predictions for real impedance are generated based on this data as depicted in Figure 7. From these predictions, the Root Mean Square Error (RMSE) value is calculated. RMSE serves as one of the two fundamental performance metrics, measuring the average difference between expected and actual values, and providing an estimate of the model's predictive accuracy. According to the RMSE values as tabulated in Table 4, the Gated Recurrent Unit (GRU) architecture seems to outperform the Long Short-term Memory (LSTM) architecture in this scenario. The lower RMSE value is, the better a given model is able to fit the dataset. Determination of RMSE value depends on the range of the observed value. In other words, RMSE represents the square root of the variance of the residuals. The GRU yields a RMSE of 57.7840, compared to the LSTM's RMSE of 61.5968. The GRU model exhibits a lower error rate than the LSTM model. Overall, the GRU architecture consistently achieves lower RMSE values, indicating superior prediction accuracy for the dataset in question. This advantage may stem from the simpler structure of GRUs, which could be more effective for this particular task.

GRU has a simpler architecture compared to LSTMs or Long Short-term Memory networks, as they feature fewer gates specifically, update and reset gates. This streamlined structure allows GRUs to train faster and require less computational power. Despite their simplicity, GRUs can perform as well as LSTMs on certain tasks, particularly when the dataset is not overly complex (Zhang *et al.*, 2018). LSTM has a more complex structure compared to other neural networks, featuring three gates: Input, output, and forget gates along with a cell state. The complex structure of LSTMs enables them to excel at capturing long-term dependencies within data. This capability is essential for tasks where context from earlier points in the sequence plays a significant role. Therefore, LSTMs generally achieve better performance on complex tasks and datasets because of their capability to preserve information over long sequences (Shi *et al.*, 2015; Mendizabal *et al.*, 2025).

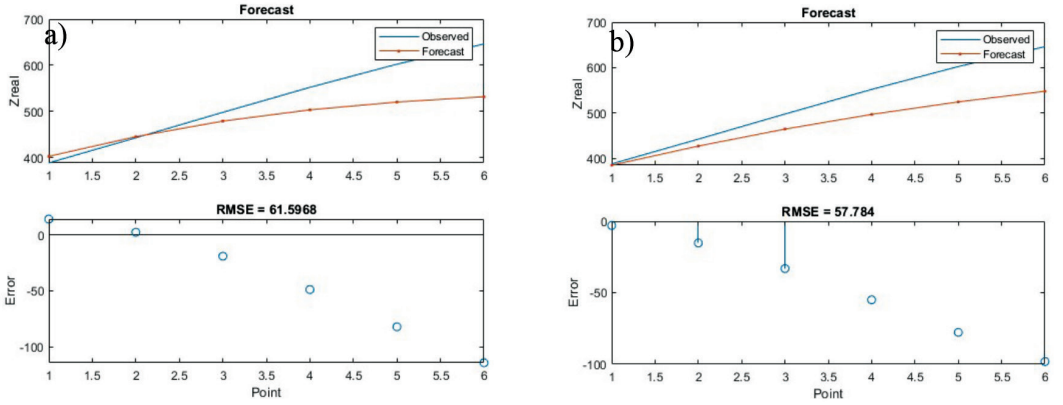

Figure 7: A forecast and observe plot with RMSE for (a) LSTM (b) GRU

Table 4: Performance indicator value of LSTM and GRU training architecture

Training Architecture	RMSE
GRU	57.7840
LSTM	61.5968

Conclusion

This study establishes CMC in combination with ionic liquids as an effective corrosion inhibitor meant for mild steel in seawater, offering practicality for both environmental and industrial field. Spectroscopic analysis via FTIR confirmed strong molecular interactions that underpin the stability of the inhibitor film. Electrochemical evaluations revealed the highest inhibition efficiency up to 94% at 40 to 60 ppm, validating the protective capability of CMC-based inhibitor. Beyond this concentration, a slight decline in efficiency was noted, likely due to destabilisation or oversaturation effects. Importantly, predictive modelling using RNNs demonstrated GRU's superior accuracy, underscoring the novelty of integrating machine learning with corrosion science. These findings validate both the experimental outcomes and the applicability of machine learning in corrosion science. Overall, this work bridges green chemistry and intelligent computation modelling, paving the way for future sustainable solution against marine corrosion.

Acknowledgements

The authors would like to express their gratitude to the Ministry of Higher Education Malaysia for funding this research via Fundamental Research Grant Scheme (FRGS), grant number FRGS/1/2020/STG05/UMT/03/1.

Conflict of Interest Statement

The authors agree that this research was conducted in the absence of any self-benefits, commercial, or financial conflicts and declare absence of conflicting interests with the funders.

References

Abdel-Gaber, A. M., Rahal, H. T., & Beqai, F. T. (2020). Eucalyptus leaf extract as an eco-friendly corrosion inhibitor for mild steel in sulfuric and phosphoric acid solutions. *International Journal of Industrial Chemistry*, *11*, 123–132. https://doi.org/https://doi.org/10.1007/s40090-020-00207-z

Abdel-Gaber, A. M., Rahal, H. T., Thebian, N., & Younes, G. (2024). Experimental and theoretical chemical studies of linalool and caffeine as corrosion inhibitors for mild steel in sulfuric acid solutions. *Biointerface Research in Applied Chemistry*, *14*(1), 1–12. https://doi.org/10.33263/BRIAC141.003

Akhlaq, M., Mushtaq, U., Naz, S., & Uroos, M. (2023). Carboxymethyl cellulose-based materials as an alternative source for sustainable electrochemical devices: A review. *RSC Advances*, *13*(9), 5723–5743. https://doi.org/10.1039/D2RA08244F

Anita, N., Joany, R. M., Dorothy, R., Aslam, J., Rajendran, S., Subramania, A., Singh, G., & Verma, C. (2023). Linear polarisation resistance (LPR) technique for corrosion measurements. In Aslam, J., Verma, C., & Hussain, C. M. (Eds.), *Electrochemical and analytical techniques for sustainable corrosion monitoring* (pp. 59–80). Elsevier. https://doi.org/10.1016/B978-0-443-15783-7.00005-0

Ariffin, A. H., Nik, W. M. N. W., Abdullah, S., Isa, M. I. N. M., Izionworu, V., & Zulkifli, M. F. R. (2024). Corrosion inhibition study of carboxymethyl cellulose-ionic liquid via electrochemical and machine learning. *Malaysian Journal of Analytical Sciences*, *28*(2), 265–276.

Arora, R. (2019). Adsorption of heavy metals–A review. *Materials Today: Proceedings*, *18*, 4745–4750.

Aslam, R., Mobin, M., Zehra, S., & Aslam, J. (2022). A comprehensive review of corrosion inhibitors employed to mitigate stainless steel corrosion in different environments. *Journal of Molecular Liquids*, *364*, 119992.

El-Housseiny, S., Abdel-Gaber, A. M., Rahal, H. T., & Beqai, F. T. (2022). Eco-friendly corrosion inhibitor for mild steel in acidic media. *International Journal of Corrosion and Scale Inhibition*, *11*(4), 1516–1538.

Ghimire, S., Deo, R. C., Wang, H., Al-Musaylh, M. S., Casillas-Pérez, D., & Salcedo-Sanz, S. (2022). Stacked LSTM sequence-to-sequence autoencoder with feature selection for daily solar radiation prediction: A review and new modeling results. *Energies*, *15*(3), 1061. https://doi.org/10.3390/en15031061

Habeeb, H. J., Luaibi, H. M., Dakhil, R. M., Kadhum, A. A. H., Al-Amiery, A. A., & Gaaz, T. S. (2018). Development of new corrosion inhibitor tested on mild steel supported by electrochemical study. *Results in Physics*, *8*, 1260–1267. https://doi.org/10.1016/j.rinp.2018.02.015

Haque, J., Zulaikha, M. A., Nik, W. W., Daoudi, W., Berdimurodov, E., & Zulkifli, F. (2023). *Alocasia odora* extract as environmentally benign corrosion inhibitor for aluminum in HCl. *Moroccan Journal of Chemistry*, *11*(4), 1013–1026. https://doi.org/10.48317/IMIST.PRSM/morjchem-v11i04.41618

Hossain, N., Asaduzzaman Chowdhury, M., & Kchaou, M. (2021). An overview of green corrosion inhibitors for sustainable and environment friendly industrial development. *Journal of Adhesion Science and Technology*, *35*(7), 673–690. https://doi.org/10.1080/01694243.2020.1816793

Huang, L., Chen, W. Q., Wang, S. S., Zhao, Q., Li, H. J., & Wu, Y. C. (2022). Starch, cellulose and plant extracts as green inhibitors of metal corrosion: A review. *Environmental Chemistry Letters*, *20*(5), 3235–3264. https://doi.org/10.1007/s10311-022-01400-5

Huang, R., Wei, C., Wang, B., Yang, J., Xu, X., Wu, S., & Huang, S. (2022). Well performance prediction based on long short-term memory (LSTM) neural network. *Journal of Petroleum Science and Engineering*, *208*, 109686. https://doi.org/10.1016/j.petrol.2021.109686

Khamis, E., Abdel-Gaber, A. M., Morshidy, M., & Mohamed, M. E. (2025). Eco-friendly inhibitors for sustainable corrosion

protection of mild steel under oilfield acidizing conditions. *Scientific Reports*, *15*, 42549. https://doi.org/10.1038/s41598-025-27271-8

Khamis, E., El-Rafey, E., Gaber, A. M. A., Hefnawy, A., El, N. G. E. D. S., & Ahmed, M. S. E. D. E. (2016). Comparative study between green and red algae in the control of corrosion and deposition of scale in water systems. *Desalination and Water Treatment*, *57*(50), 23571–23588. https://doi.org/10.1080/19443994.2015.1135480

Kim, H. J. (2023). Spectroscopic and chemical properties of ionic liquids: Computational study. *The Chemical Record*, *23*(8), e202300075. https://doi.org/10.1002/tcr.202300075

Koch, G., Varney, J., Thompson, N., Moghissi, O., Gould, M., & Payer, J. (2016). *NACE 2016 impact study. International measures of prevention, application, and economics of corrosion technologies study*. http://impact.nace.org/documents/Nace-International-Report.pdf

Lazanas, A. C., & Prodromidis, M. I. (2023). Electrochemical impedance spectroscopy—Atutorial.*ACSMeasurement Science Au*, *3*(3), 162–193. https://doi.org/10.1021/acsmeasuresciau.2c00070

Lipu, M. H., Ansari, S., Miah, M. S., Meraj, S. T., Hasan, K., Shihavuddin, A. S. M., Hannan, M. A., Muttaqi, K. M., & Hussain, A. (2022). Deep learning enabled state of charge, state of health and remaining useful life estimation for smart battery management system: Methods, implementations, issues and prospects. *Journal of Energy Storage*, *55*, 105752. https://doi.org/10.1016/j.est.2022.105752

Liu, T., Lyu, W., Li, Z., Wang, S., Wang, X., Jiang, J., & Jiang, X. (2023). Recent progress on corrosion mechanisms of graphene-reinforced metal matrix composites. *Nanotechnology Reviews*, *12*(1), 20220566. https://doi.org/10.1515/ntrev-2022-0566

Macedo, R. G. M. D. A., Marques, N. D. N., Paulucci, L. C., Cunha, J. V. M., Villetti, M. A., Castro, B. B., & Balaban, R. D. C. (2019). Water-soluble carboxymethylchitosan as green scale inhibitor in oil wells. *Carbohydrate Polymers*, *215*, 137–142.

Mendizabal, J., Vernon, D., Martin, B., Bajón-Fernández, Y., & Soares, A. (2025). Short-term memory artificial neural network modelling to predict concrete corrosion in wastewater treatment plant inlet chambers using sulphide sensors. *Journal of Water Process Engineering*, *69*, 106821.

Nik, W. W., Ravindran, K., Al-Amiery, A. A., Izionworu, V. O., Fayomi, O. S. I., Berdimurodov, E., Daoudi, W., Zulkifli, F., & Dhande, D. Y. (2023). *Piper betle* extract as an eco-friendly corrosion inhibitor for aluminium alloy in hydrochloric acid media. *International Journal of Corrosion and Scale Inhibition*, *12*(3), 948–960.

Olajire, A. A. (2017). Corrosion inhibition of offshore oil and gas production facilities using organic compound inhibitors—A review. *Journal of Molecular Liquids*, *248*, 775–808.

Pine Research Instrumentation. (2016, April). *Linear polarization resistance and corrosion rate - theory and background* (p. 1).

PourghasemiHanza, A., HosseinpourRokni, M., Naderi, R., Kowsari, E., & Mousavi, M. (2021). An imidazole-based benzilic-dicationic ionic liquid performance in 1.0 M HCl solution to mitigate the mild steel degradation: Electrochemical noise/impedance investigation. *Journal of Molecular Liquids*, *336*, 116320.

Pruthviraj, R. (2016). Corrosion studies of AA2024 in sea water using sodium benzoate as an inhibitor. *Journal of Material Science & Engineering*, *5*, 2169–0022.

Rahman, M. S., Hasan, M. S., Nitai, A. S., Nam, S., Karmakar, A. K., Ahsan, M. S., Shiddiky, M. J., & Ahmed, M. B. (2021).

Recent developments of carboxymethyl cellulose. *Polymers*, *13*(8), 1345.

Reza, N. A., Akhmal, N. H., Fadil, N. A., & Taib, M. F. M. (2021). A review on plants and biomass wastes as organic green corrosion inhibitors for mild steel in acidic environment. *Metals*, *11*(7), 1062.

Saheed, I. O., Azeez, S. O., & Suah, F. B. M. (2022). Imidazolium based ionic liquids modified polysaccharides for adsorption and solid-phase extraction applications: A review. *Carbohydrate Polymers*, *298*, 120138.

Shi, X., Chen, Z., Wang, H., Yeung, D. Y., Wong, W. K., & Woo, W. C. (2015). Convolutional LSTM network: A machine learning approach for precipitation nowcasting. *Advances in Neural Information Processing Systems*, *28*.

Sohaimy, M. I. H. A., Yusof, Y., & Isa, M. I. N. M. (2022). Improving ionic conductivity of carboxymethyl cellulose solid biopolymer electrolyte with assist from dimethyl carbonate. *Trends in Sciences*, *19*(19), 6174. https://doi.org/10.48048/tis.2022.6174

Solmaz, R., Salcı, A., Dursun, Y. A., & Kardaş, G. (2023). A comprehensive study on the adsorption, corrosion inhibition efficiency and stability of acriflavine on mild steel in 1 M HCl solution. *Colloids and Surfaces A: Physicochemical and Engineering Aspects*, *674*, 131908. https://doi.org/10.1016/j.colsurfa.2023.131908

Thiyagalingam, J., Shankar, M., Fox, G., & Hey, T. (2022). Scientific machine learning benchmarks. *Nature Reviews Physics*, *4*(6), 413–420. https://doi.org/10.1038/s42254-022-00441-7

Umoren, S. A., AlAhmary, A. A., Gasem, Z. M., & Solomon, M. M. (2018). Evaluation of chitosan and carboxymethyl cellulose as ecofriendly corrosion inhibitors for steel. *International Journal of Biological Macromolecules*, *117*, 1017–1028. https://doi.org/10.1016/j.ijbiomac.2018.06.014

Verma, C., Alfantazi, A., & Singh, V. (2024). Cellulose, cellulose derivatives, nanocellulose and cellulose composites in sustainable corrosion protection: Challenges and opportunities. *Physical Chemistry Chemical Physics*, *26*, 11217-11242. https://doi.org/10.1039/D3CP06057H

Voloshin, A., Nifantiev, N., Egorov, M., Alimbekov, R., & Dokichev, V. (2021, October). Development and implementation of green inhibitors of gas hydrate formation in the fields of Western Siberia. In *SPE Russian Petroleum Technology Conference* (p. D031S014R003). SPE. https://doi.org/10.2118/206470-MS

Wadhwani, P. M., Panchal, V. K., & Shah, N. K. (2016). Investigation of anti-corrosive properties of *o*-anisidine-*N*-salicylidene and its nanocomposite *o*-anisidine-*N*-salicylidene/NiONPs on mild steel in 2 N HCl. *RSC Advances*, *6*(93), 90897–90915. https://doi.org/10.1039/C6RA13630C

Yesudass, S., Olasunkanmi, L. O., Bahadur, I., Kabanda, M. M., Obot, I. B., & Ebenso, E. E. (2016). Experimental and theoretical studies on some selected ionic liquids with different cations/anions as corrosion inhibitors for mild steel in acidic medium. *Journal of the Taiwan Institute of Chemical Engineers*, *64*, 252–268. https://doi.org/10.1016/j.jtice.2016.04.006

Zhang, D., Hølland, E. S., Lindholm, G., & Ratnaweera, H. (2018). Hydraulic modeling and deep learning based flow forecasting for optimizing inter catchment wastewater transfer. *Journal of Hydrology*, *567*, 792–802. https://doi.org/10.1016/j.jhydrol.2017.11.029

Zhang, J., Zou, D., Zhai, S., Yan, Y., Yang, H., He, C., Ke, Y., Singh, S., & Cheng, G. (2022). Enhancing the interaction between cellulose and dilute aqueous ionic liquid solutions and its implication to ionic liquid recycling and reuse. *Carbohydrate Polymers*, *277*, 118848. https://doi.org/10.1016/j.carbpol.2021.118848

Zhang, R., Sur, D., Li, K., Witt, J., Black, R., Whittingham, A., Scully, J. R., & Hattrick-Simpers, J. (2024). Bayesian assessment of commonly used equivalent circuit models for corrosion analysis in electrochemical impedance spectroscopy. *npj Materials Degradation*, *8*(1), 120. https://doi.org/10.1038/s41529-024-00537-8

Zheng, H., Zhang, B., Wang, X., Lu, Y., Li, F., & Li, C. (2023). Improved corrosion resistance of carbon steel in soft water with dendritic-polymer corrosion inhibitors. *Chemical Engineering Journal*, *452*, 139043. https://doi.org/10.1016/j.cej.2022.139043

Zhong, S., Zhang, K., Bagheri, M., Burken, J. G., Gu, A., Li, B., Ma, X., Marrone, B. L., Ren, Z. J., Schrier, J., & Shi, W. (2021). Machine learning: New ideas and tools in environmental science and engineering. *Environmental Science & Technology*, *55*(19), 12741–12754. https://doi.org/10.1021/acs.est.1c01339

Zulkifli, M. F. R., Bahrin, S. N. S., Abdullah, S., Ghazali, M. S. M., Norsani, W. M., & Nik, W. (2021). *Citrus aurantifolia* leaf extract as a potential anti-corrosion additive in alkyd paint for mild steel. *Journal of Sustainability Science and Management*, *16*(3), 10–20. https://doi.org/10.46754/JSSM.2021.04.002